

Effect of transparent Pb substrates on the structural, optical, dielectric and electrical properties of copper selenide thin films

A. F. Qasrawi^{a,b,*}, A. N. Abu Ghannam^a

^a*Department of Physics, Arab American University, Jenin, Palestine*

^b*Department of Electrical and Electronics Engineering, Istinye University, 34010, Istanbul, Turkey*

Herein, copper selenide thin films are coated onto transparent lead substrates. Pb/CuSe stacked layers is fabricated by the thermal evaporation technique under a vacuum pressure of 10^{-5} mbar. They are structurally, morphologically, optically and electrically characterized. Lead substrates enhanced the crystallinity of CuSe through increasing the crystallite sizes, reducing the microstrain and lowering defect densities. In addition, a blue shift in the energy band gap associated with remarkable increase in the value of the high frequency dielectric constant resulted from replacement of glass by Pb substrates. Moreover, significant increase in the optical conductivity in the ultraviolet range of light is observed. Fitting the optical conductivity in accordance with Drude- Lorentz models allowed determining the effect of transparent Pb substrates on the plasmon frequency, scattering time at femtosecond level and drift mobility of CuSe. On the other hand, electrical measurements on the Pb/CuSe/C by imposing an ac signal of low amplitude in the frequency domain of 10-1000 MHz, have shown that the Pb/CuSe can perform as negative capacitance source employable for devices scaling and low power applications.

(Received December 11, 2021; Accepted March 1, 2022)

Keywords: Pb/CuSe interfaces, X-ray diffraction, Optical conductions, Negative capacitance

1. Introduction

Recently, lead substrates in thin film form has attracted the attention for their ability to enhance the performance of optoelectronic devices. As for examples, coating ZnO films onto Pb thin film substrates are employed to assess the feasibility of achieving a low dose gamma (Co-60) irradiation detector [1]. The ZnO/Pb/gate device which behaved as a metal oxide semiconductor fields effect transistors (MOSFET) was able to detect low doses of gamma irradiation (up to 12.98 μ SV). In addition, lead ions are also mentioned playing central role in enhancing the fluorescence of Ag₂S Quantum dots [2]. These quantum dots were found attractive for use in bio-sensing issues [2]. Moreover, introducing Pb ion into copper selenide lattice successfully improved the thermoelectric properties and the stability of the compound [3]. Particularly, the thermoelectric power of copper selenide is improved by 22.5% at 800 K. In the same context, copper selenide thin films are mentioned good candidates for fabrication of photovoltaic devices [4, 5]. This material is reported displaying photoluminescence characteristics in the near ultraviolet-blue region. As a *p*-type semiconductor, CuSe is mentioned having excellent electrical and optical properties [5]. However, because they show wide energy band gap they are not sensitive to visible light irradiation. CuSe is known to exhibit different crystallographic shapes including tetragonal, monoclinic, hexagonal and cubic [5]. In nanoscale form CuSe is applicable in electric, thermal and photovoltaic device production. It can operate under mild conditions of temperature and pressure [5].

The above mentioned features of Pb as substrates and as doping agents and their effective role on copper selenide motivated us to study the features of layers of CuSe thin films coated onto Pb substrates. For this reason, here in this work, we have coated copper selenide thin films onto transparent (100 nm thick)/nontransparent (1.0 μ m thick) layers of Pb films. The glass/CuSe and Pb/CuSe films are studied by means of X-ray diffraction, optical spectrophotometry and

* Corresponding author: atef.qasrawi@aaup.edu
<https://doi.org/10.15251/CL.2022.193.163>

impedance spectroscopy techniques. The measurements allowed exploring the effect of Pb on the crystalline nature, lattice constants and defect densities, morphology, optical absorbability, energy band gaps and dielectric dispersion. The role of Pb substrates on the optical conductivity parameters including the critical oscillator energies, the drift mobility values, scattering times at femtosecond levels and plasmon frequencies are also discussed. In addition, the properties of the Pb/CuSe/C devices as negative capacitance sources in the microwave frequency domain is explored.

2. Experimental details

Lead substrates of thicknesses of 100 nm are grown onto chemically and ultrasonically cleaned glass substrates using a vacuum thermal evaporation system (NORM VCM-600). The vacuum pressure is kept at $\sim 10^{-5}$ mbar. The source material is lead micro-powders (99.999%, Alpha Aesar). The freshly produced lead films are covered with a 1.0 μm thick copper selenide (99.99%, Alpha Aesar) using NORM VCM-600 under a vacuum pressure of $\sim 10^{-5}$ mbar. Some of the CuSe samples of thicknesses of 1.0 μm were produced onto glass to allow exploring the Pb effects. The *p*-type conductivity of CuSe was determined by the hot probe technique. The hot probe technique was employed for glass/CuSe samples only. For the ac electrical measurements, some of the Pb substrates were made thicker (1.0 μm) to assure good electrical contacts. Pb/CuSe films were masked with circular masks of areas of $3.14 \times 10^{-2} \text{ cm}^2$ to produce carbon point contacts on the top surface of CuSe layer. The film thicknesses were measured with the help of an in situ monitoring Inficon STM-2 thickness monitors. The X-ray diffraction (XRD) patterns were recorded with the help of a MiniFlex 600 XRD system. The $\theta - 2\theta$ scan was carried out in the range of $10-70^\circ$ in 0.05 and 0.02 steps at speed of $0.5^\circ/\text{min}$. The minimum step width of the XRD system is $2\theta = 0.005^\circ$. The optical transmittance and reflectance spectra at normal incidence were measured with the help of Thermoscientific Evolution 300 spectrophotometer equipped with Pike VEE MAX II reflectometer. The conductance and capacitance spectra in the microwave frequency domain were recorded with the help of Agilent 4291B 1.0 M–1.8 GHz impedance analyzer.

3. Results and discussion

Images of copper selenide thin films coated onto glass and transparent Pb substrates of thicknesses of 100 nm are presented in inset-1 of Fig.1. The optical images indicate slight changes in the samples colors. On the other hand, the X-ray diffraction patterns (XRD) of copper selenide which is grown onto glass and lead substrates are shown in Fig.1. In accordance with the observed XRD patterns, thin films of copper selenide are of polycrystalline nature. All the observed peaks are indexed in accordance with the cubic phase of copper selenide (PDF card No: 01-071-4325) except for one peak detected at 24.45° . This peak is most probably assigned to orthorhombic CuSe ((PDF card no: 2027-0184). The calculated phase weight of orthorhombic CuSe ($W_{ph} = \frac{\sum A_{hkl-\text{orth.-CuSe}}}{\sum A_{hkl}}$; A is area of the peak) in the films is 17.59% and 19.31%, for glass/CuSe and Pb/CuSe, respectively. In addition, the lattice parameters of the cubic phase of the glass/CuSe and Pb/CuSe are found to be $a = 5.697 \text{ \AA}$ and 5.676 \AA , respectively. The currently reported a values are close to those reported in literature [6-8]. It can also be noted from Fig. 1 that the maximum of the reflection peaks of Pb (JCPDS standard card (004- 0686)) is centered at same diffraction angle ($2\theta = 31.15^\circ$) of cubic CuSe. The coincidence of the two angles make detection of Pb peaks in the XRD patterns of Pb/CuSe not possible.

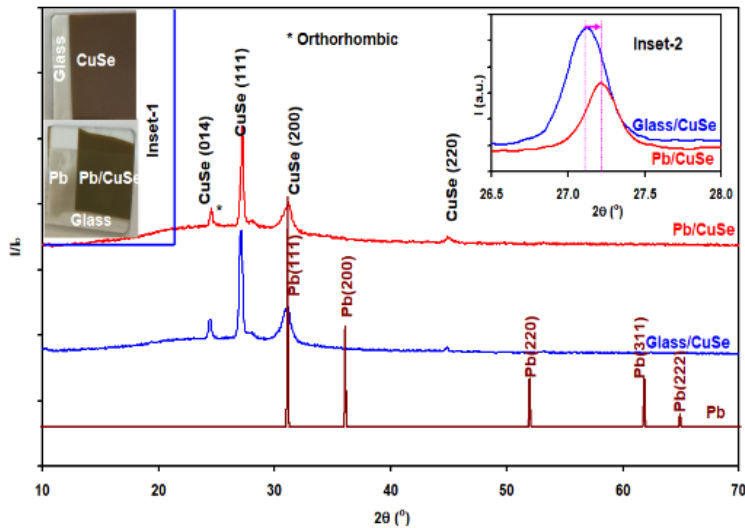


Fig. 1. the X-ray diffraction peaks for Pb, glass/CuSe and Pb/CuSe thin films. Inset-1 shows the optical images for the CuSe films and inset-2 is an enlargement of the maximum peak.

Inset-2 of Fig.1, clearly illustrate the effect of Pb substrates on the structural properties of copper selenide. Namely, the maximum peak of CuSe are shifted to the right resulting in higher 2θ values. The intensity of the peak also decreased. Even though the intensity decreased, the full wave half maximum of the peak decreased from $\beta = 0.30^\circ$ to $\beta = 0.25^\circ$ indicating less broadening of the peak after using Pb. The calculated crystallite size ($D = \frac{0.94\lambda}{\beta \cos\theta}$; β : peak broadening [4, 9]), microstrain ($\varepsilon = \frac{\beta}{4 \tan\theta}$ [9]), staking faults ($SF\% = \frac{2\pi^2\beta}{45\sqrt{3}\tan(\theta)}$ [9]), dislocation density ($\delta = \frac{15\varepsilon}{aD}$ [9]) and stress ($S = \gamma \varepsilon$; $\gamma = 62$ GPa [10]) which are shown in Table-1 are highly affected by the Pb substrates. Particularly, an increase in the crystallite size associated with decrease in the microstrain, in the stress, in the stacking faults percentages and in the defect density is achieved after replacement of glass by transparent Pb substrates.

Table. 1 Mechanical properties of glass/CuSe and Pb/CuSe.

	a (Å)	D (nm)	$\varepsilon \times 10^{-3}$	$S \times 10^9$ dyne/cm ²	SF%	$\delta \times 10^{11}$ line/cm ²
glass/CuSe	5.697	28	5.432	3.368	0.270	5.02
Pb/CuSe	5.676	33	4.689	2.907	0.216	3.77

Fig. 2 (a) and (b) show the scanning electron microscopy (SEM) images for the films coated onto glass and Pb substrates, respectively. CuSe films coated onto glass substrates display rods shaped randomly distributed grains being impeded in an amorphous sea of CuSe. The average diameter and length of the rod like grains are 125 nm and 1.20 μ m, respectively. On the other hand, the SEM images for the Pb substrates which are presented in the inset of Fig. 2 (b) display mostly rectangular grains of averages sizes of 265 nm. Coating CuSe onto Pb (Fig. 2 (b)) resulted in very dense and well distributed rectangular grains of average sizes of ~ 410 nm. For most of the dark-grey appearing grains, a bright tiny grain appears on it. These bright colored grains have averages size of ~ 96 nm. Recalling that the grain is composed of group of crystallites, then the grain growth is assigned to the increased crystallite sizes in the presence of Pb. To get information about the composition of the grains, the energy dispersive X-ray analysis were carried out by selecting points and areas on bright grains and on dark grey-colored grains as well as on rod

shaped grains. In general, the composition of the grains is homogeneous and the atomic percentages vary by 2-5% of the measured value at maximum. The EDS spectra which are illustrated in Fig. 2 (c) indicate the presence of glass ($\text{SiO}_2\text{:MgO}\text{:Na}_2\text{O}\text{:CaO}$), Au, Pb and CuSe. No other elements are detected in the spectra. Au is presented because it was used to prevent electron contaminations. The numerical analysis on points and areas selected from various samples carried out in the same evaporation cycle and/or different evaporation cycles revealed that CuSe films coated onto glass substrates are composed of 54.37 at. % Cu and 45.62 at.% Se, resulting in formation of $\text{Cu}_{1.19}\text{Se}$. Copper selenide films coated onto Pb substrates contained 51.18 at.% Cu and 48.82 at. % Se revealing the chemical formula $\text{Cu}_{1.05}\text{Se}$. The numerical data of EDS suggest that the presence of Pb reduced the amount of excess Cu in the samples. The stoichiometry of the composition is enhanced when glass is replaced by Pb substrates. On possible reason for the improvements in compositional stoichiometry, the crystallite and grain sizes that is accompanied with less microstrain, less stress and less defect density is the ionic substitutions of Pb^{+4} ions (94 pm) in irregularly distributed vacant sites of Cu^{+1} (98 pm) [11, 12]. The change in the shape of the grains upon coating copper selenide onto metals substrates was also observed for Cu/CuSe films. It is mentioned that for a monolayer of CuSe deposited onto a Cu substrate, strain relaxation lead to periodic patterns of triangular nanopores with uniform sizes [13]. In addition, compared to CuSe films coated onto oxide substrates (MoO_3), Pb substrates allowed achieving higher crystallite sizes, less defect densities and much less microstrains [14].

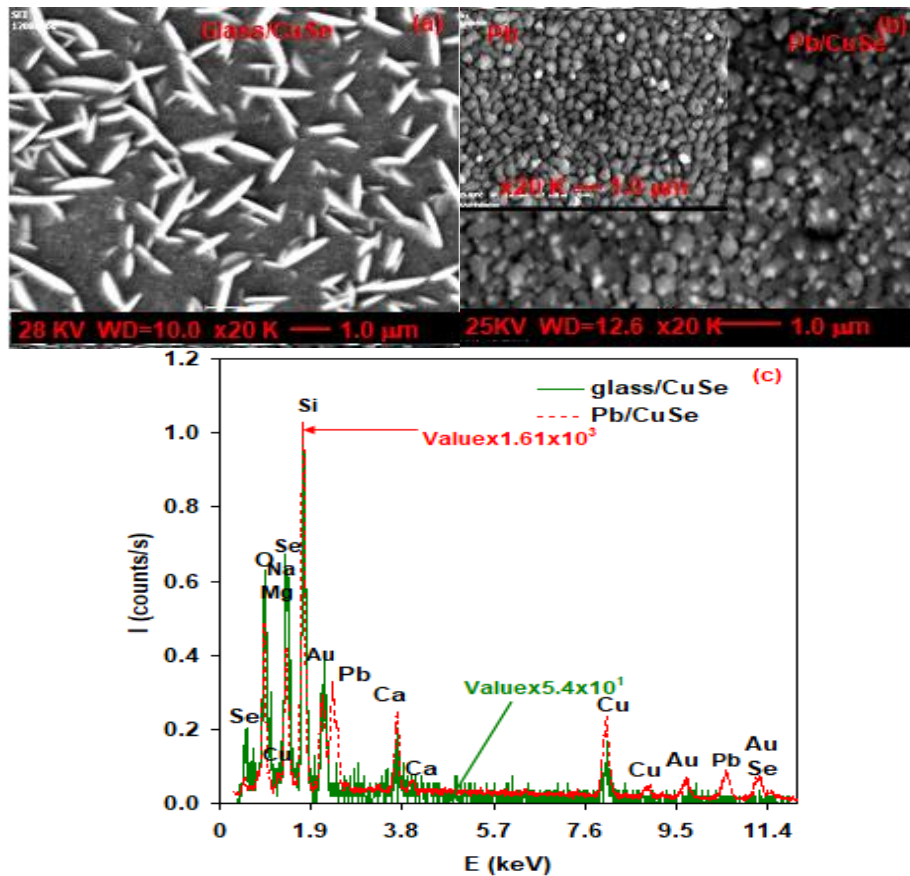


Fig. 2. The scanning electron microscopy images for (a) glass/CuSe and (b) Pb/CuSe films. (c) the energy dispersive X-ray spectra from (glass, Pb)/CuSe films. Inset of (b) show the SEM images for Pb films.

To observe the effect of transparent Pb substrates on the optical and dielectric properties of CuSe. The transmittance (T) and reflectance (R) of copper selenide thin films, were recorded in the spectra range of 4.0-1.1 eV. As illustrated in Fig. 3 (a), no significant effect of the transparent Pb substrate on the transmittance of CuSe can be observed. This is may be due to the high

transparency of glass/Pb films (Fig. 3 (a)). However, the changes in the reflectance of glass/Pb, Pb/CuSe are more pronounced than that of glass/CuSe. T and R spectra are used to obtain information about the absorption coefficient (α) spectra through the relation [14],

$$T = \frac{(1-R_{glass})(1-R_{Pb})(1-R_{Pb/CuSe})e^{-\alpha t}}{1-R_{glass}R_{Pb}R_{Pb/CuSe}e^{-3\alpha t}}. \quad (1)$$

Here, t is the sample thickness. The absorption coefficient spectra for glass/CuSe and Pb/CuSe, which are illustrated in Fig. 3 (b), show that the absorption coefficient spectra follows four regions of absorption in the studied range of incident photon energy. Namely, the absorption coefficients decrease with decreasing incident photon energy (E) in the range of 4.0-3.20 eV (first region) reaching an absorption saturation in the second region (3.20-2.78 eV). It, then, sharply decay in the third region (2.78-1.81 eV). In the fourth region of absorption (1.80-1.14 eV), the absorption coefficient increases with decreasing incident photon energy. The increase of α values with decreasing photon energy result from the domination of free carrier absorption mechanism. Free carrier absorption is due to the lattice distortion effect that arises from dislocations and impurities that changes the electric dipole moment [20]. As the light wavelength increases in the IR region, they become able to reach the lattice and can then excite phonons. The excited phonons interact with electrons/holes and sets these charge carriers free allowing enhanced absorption in IR region [15].

Employing Tauc's equation $(\alpha E)^2 \propto (E - E_g)$ [14, 15] in third and first regions of $\alpha - E$ variations permit calculating the energy band gaps (E_g) of glass/CuSe and Pb/CuSe films. The linear fittings of the $(\alpha E)^2 - E$ variations which are shown in Fig. 3 (c) and (d) crosses the E -axis at $E = E_g^1 = 2.82$ eV and at $E = E_g^1 = 3.08$ eV and at $E = E_{g-glass/CuSe}^3 = 2.30$ eV and $E = E_{g-Pb/CuSe}^3 = 2.33$ eV, for glass/CuSe and Pb/CuSe, and respectively. The superscripts 1 and 3 of the symbol E_g relates to first and third absorption regions, respectively. The obtained energy band gap of glass/CuSe is consistent with literature data [16]. The replacement of glass by transparent Pb substrates increased the energy band gap by 260 meV in the first region and by 30 meV in the third region. An increase in the energy band gaps values of CuSe was also observed when CuSe was coated onto oxide substrates [14]. Published works [17] shows that the presence of lead as a dopant agent increases the band gap for copper selenide and decreases its absorption coefficient, the amount of change depends on the doping concentration of lead. CuSe films are previously observed exhibiting two energy band gaps due to the two dimensional transitions property of the Cu (3d) and Se (4p) states [18]. The valence bands maxima of CuSe is formed from the antibonding of the Cu (3d) and Se (4p) orbital states. The conduction band minima are formed due to the antibonding of Se (4p) orbitals [18]. The increase in the value of the energy band gap is probably assigned to the quantum size effect in the crystallites (or grains) [19].

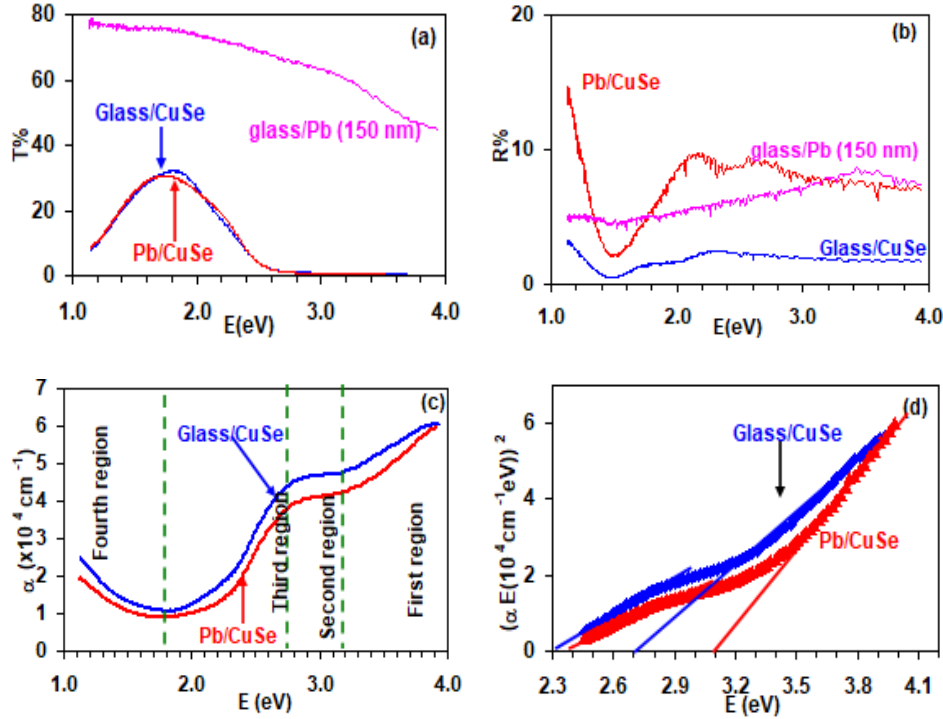


Fig. 3. The optical (a) transmittance, (b) the reflectance, (c) absorption coefficient spectra and (d) the Tauc's equation fitting in the visible and ultraviolet ranges for (glass, Pb)/CuSe films.

The effect of transparent Pb substrates on the dielectric constant (ϵ_r) and on the optical conductivity ($\sigma(w) = \epsilon_{im}w/4\pi$; $w = 2\pi c/\lambda$) is evident from Fig. 4 (a) and (b), respectively. The effective dielectric constant (ϵ_{eff}) is calculated from the measured reflectance at normal incidence and calculated absorption coefficient using the relation [14, 20],

$$R = \frac{(\sqrt{\epsilon_{eff}} - 1)^2 + k^2}{(\sqrt{\epsilon_{eff}} + 1)^2 + k^2} \quad (2)$$

Here, $k = \alpha\lambda/(4\pi)$ is the extinction coefficient. ϵ_r and ϵ_{im} are calculated using the relations, $\epsilon_r = \epsilon_{eff} - k^2$ and $\epsilon_{im} = 2\sqrt{\epsilon_{eff}}k$. It is clear from Fig. 4 (a), that the real part of the dielectric constant highly increased upon replacing glass substrates by Pb substrates. Particularly, in the high energy range of spectra, the high frequency dielectric constant (ϵ_∞) increase from 1.78 to 3.05 (at $E=3.0$ eV, as an example). In the IR range of light ($E < 1.40$ eV), $\epsilon_r - E$ variations of Pb/CuSe follow sharper trends of variation compared to that of glass/CuSe. Namely, while $\epsilon_r = 8.43E^{-4.13}$ for Pb/CuSe, $\epsilon_r = 2.54E^{-1.74}$ for glass/CuSe. The nonlinear dependence of ϵ_r on energy ($E = \frac{hc}{\lambda}$) indicates the possibility of employing the (glass, Pb)/CuSe for nonlinear optical applications [20, 21, 22]. The dielectric spectra of glass/CuSe and Pb/CuSe, additionally, display broaden peaks centered at critical energy values of 2.30 and 1.82 eV and at 2.60 and 2.12 eV, respectively. The value of critical energy being 2.30 eV, corresponds to the direct allowed transitions energy band gap of CuSe. The critical energy value being 1.82 eV appears as a result of transitions from the valence band centered at $R_{3,4v}$ of the first Brillouin zone of selenium to the conduction band centered at H_{6c} of the first Brillouin zone of Se [23]. The peak centered at 2.12 eV also corresponds to transitions originating from H_{6v} to H_{6c} in selenium [23]. The peak which is detected at 2.60 eV can be assigned to the transitions from the valance band maxima (VBM) derived from antibonding of Cu-Se states. It is mentioned that transitions from the nonbonding Cu (3d) states with nondispersive character centered at 2 eV below the VBM to a roughly 1-eV wide density of states gap centered at 2.6 eV [24].

On the other hand, the optical conductivity spectra which are calculated from the imaginary part of the dielectric (ε_{im}) spectra for (glass, Pb)/CuSe are shown in Fig. 4 (b). In accordance with the figure for all incident photon energies larger than 2.70 eV the optical conductivity is increased remarkably as a result of replacement of glass by Pb substrates. As for examples, at $E = 3.70$ eV, $\sigma_{glass/CuSe}$ which exhibited value of $16.16 (\Omega cm)^{-1}$ increases to $19.74 (\Omega cm)^{-1}$ when Pb replaces glass. Employing Drude-Lorentz approaches for optical conduction is possible using the relation [25],

$$\sigma(w) = \sum_{i=1}^k \frac{w_{pi}^2 w^2}{4\pi\tau_i((w_{ei}^2 - w^2)^2 + w^2\tau_i^2)} . \quad (3)$$

Here, w is the radial frequency of light, $w_{pe} = \sqrt{4\pi P e^2/m^*}$ is the plasmon frequency, w_{ei} is the hole-plasmon coupled oscillator frequency, τ_i is the average scattering time at femtosecond level, P is the free hole density and $m^* = (m_{Pb}^{*-1} + m_{CuSe}^{*-1})^{-1}$ is the reduced effective mass of the Pb/CuSe system. $m_{CuSe}^* = 0.5m_o$ [14] and $m_{Pb}^* = 2.0m_o$ [25] for CuSe and for lead, respectively, are substituted into Eqn. (3). Running the series up to $k = 5$ was sufficient to reproduce the experimental data. The theoretically estimated optical conductivity is plotted by black colored circles in Fig. 4 (b). The fitting of the conductivity spectra resulted in determining the optical conductivity parameters which are presented in Table-2.

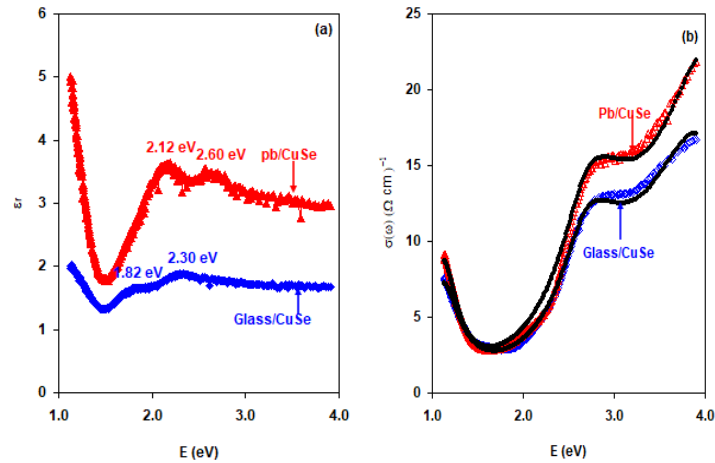


Fig. 4 (a) the real of the dielectric spectra and (b) the optical conductivity for (glass, Pb)/CuSe films. The black colored circles in (b) illustrate the solution obtained by Eqn. (3).

As illustrated in Table-2, for glass/CuSe, the dominant oscillators are centered in the infrared (IR) range at 1.11 eV, in the visible range of light (VL) at 2.69 and at 2.88 eV and in the ultraviolet range (UV) at 3.93 and 4.13 eV. Replacing glass by Pb slightly shifted the oscillators of the UV band. For the IR oscillator, replacement of glass by transparent Pb substrates increased the scattering time at femtosecond level, enhanced the drift mobility by 65.8%, decreased the free hole concentration by 25.0% and lowered the plasmon frequency by only 3.4%. The numerical data suggests that the presence of transparent lead substrates improved the performance of CuSe when employed for IR sensing issues. The gained advantage is presented by more mobile carrier transport without significant reduction in the plasmon frequency. Similar achievements are also obtained in the VL range of light. Namely, the drift mobility is enhanced by ~25.4% at 2.69 eV and by 21.6% at 2.88 eV. For the latter oscillator, the plasmon frequency is increased from 3.76 GHz to 4.70 GHz. The drift mobility and plasmon frequency values are also increased in the UV range of light without altering the scattering time and slight increase in the free hole density from $8.0 \times 10^{18} cm^{-3}$ to $8.5 \times 10^{18} cm^{-3}$. It is also interesting to mention that, while $MoO_3/CuSe$ systems are optically conductive in the IR range of light, Pb/CuSe system is more conductive in

the UV range of light [14]. The values of the drift mobility being larger than $1.0 \text{ cm}^2/\text{Vs}$ and the remarkable increase in the optical conductivity in addition to the high value of cutoff frequency (plasmon frequency) indicating that the Pb/CuSe attractive for the fabrication of UV detectors. The lack of UV sources from our laboratory tools make this test impossible. However, we located point contacts made of carbon to electrically characterize the performance of Pb/CuSe. The schematics of the Pb/p –CuSe/C devices are illustrated in inset-1 of Fig.5 (a).

Table 2. Optical conductivity parameters for glass/CuSe and Pb/CuSe films.

	Glass/CuSe					Pb/CuSe				
	IR		VL		UV	IR		VL		UV
	1	2	3	4	5	1	2	3	4	5
$E_e = \hbar w_e (\text{eV})$	1.11	2.69	2.88	3.93	4.13	1.11	2.69	2.88	4.08	4.13
$\tau_i (\text{fs})$	1.50	1.00	0.50	0.45	0.30	2.0	1.00	0.50	0.45	0.40
$p (\times 10^{18} \text{ cm}^{-3})$	8.00	7.00	20.0	53.0	8.00	6.00	5.00	25.0	53.0	8.50
$\mu (\text{cm}^2/\text{Vs})$	5.30	3.50	1.80	1.60	0.40	8.79	4.39	2.19	1.97	1.75
$w_{pi} (\text{GHz})$	2.38	2.22	3.76	6.12	2.38	2.30	2.10	4.70	6.84	2.74

As practical application to the proposed Pb/CuSe/C interfaces, we have imposed an ac signal of small amplitude between the terminals of source and gate. The resulting ac conductivity (σ_{ac}) and capacitance (C) spectra are displayed in Fig. 5 (a) and (b), respectively. The ac conductivity spectra which are studied in the frequency domain of 10-1000 MHz, decrease by more than three orders of magnitude as the frequency increase from 10 to 1000 MHz. The sharp decay of the ac conductivity indicates the domination of the correlated barriers hopping conduction (CBH) in the samples. The ac conductivity due to the correlated barrier hopping is given by the relation [26, 27],

$$\sigma_{CBH}(w) = \sigma(H) + \frac{\sigma(L)-\sigma(H)}{1+(w\tau_{hop})^2}. \quad (4)$$

In this equation, $\tau_{hop} = \tau_o \exp(\frac{E_H}{kT})$, τ_o is characteristic relaxation time which is the inverse of the phonon frequency ($v = \tau_o^{-1}$), $\sigma(L)$ and $\sigma(H)$ are the low and high frequency conductivity values, respectively. E_H is regarded as the height of potential barriers that the charge carriers hop over. By substituting the value of the longitudinal optical phonon frequency for CuSe as 260.2 cm^{-1} [28], $\tau_o = 1.3 \times 10^{-13} \text{ s}$ is identified. The experimental ac conductivity spectra which are shown by the black colored circles in Fig. 5 (a) is obtained from Eqn. (4) assuming a hopping time constant of 82.0 ns. These (τ_o, τ_{hop}) value allow determining the average height of the correlated barrier as $E_H = 0.345 \text{ eV}$. The values of $\sigma(L)$ and $\sigma(H)$ are also found to be $3.5 \times 10^{-2} (\Omega\text{cm})^{-1}$ and $1.0 \times 10^{-7} (\Omega\text{cm})^{-1}$, respectively. The good correlation between the experimentally measured and theoretically calculated ac conductivity spectra confirm the conduction by CBH.

In addition, as also illustrated in Fig. 5 (b) the capacitance is negative. Negative capacitance (NC) effects is dominant in all the studied spectral range. This feature makes the Pb/CuSe/C proposed transistors applicable as NC-field effect transistors which are beneficial for devices scaling [29] and low power operations [30]. NC effect is mentioned resulting in increased gate capacitance leading to enhanced gate controllability and improved switching characteristics [31]. One reason for the origin of the NC effect in Pb/CuSe/C could be surface charges or from minority-carrier injection caused by accumulation of minority carriers at the crystallite boundaries [9].

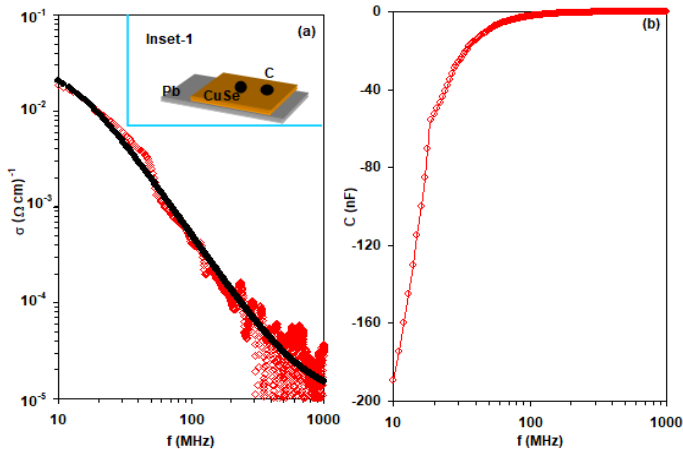


Fig. 5. (a) the conductivity spectra in the microwave frequency domain and (b) the capacitance spectra for Pb/CuSe/C devices. Inset 1 of (a) show the geometrical design of the device.

4. Conclusions

In this work, we have explored the effects of Pb substrates on the structural, morphological, optical and electrical properties of copper selenide thin films. Transparent Pb substrates of thicknesses of 100 nm successfully enhanced the crystalline phase and blueshifted the energy band gap of CuSe. In addition, remarkable enhancement in the dielectric constant values and in the optical conductivity in the ultraviolet range of light is achieved. Presenting the optical conductivity by Drude-Lorentz model allowed determining the optical conductivity parameters. These parameters suggested the applicability of the Pb/CuSe interfaces as optoelectronic devices. The devices are fabricated and tested by means of ac electrical measurements. They are observed exhibiting negative capacitance effect which is beneficial for devices scaling and low power applications.

Acknowledgements

This work was supported by the Deanship of Scientific Research (DSR), Arab American University, Jenin, Palestine and by DSR of Istinye University, Istanbul, Turkey. The authors, therefore, gratefully acknowledge the DSR technical and financial support.

References

- [1] A. M. A. Ali, N. M. Ahmed, N. A. Kabir, M. A. Almessiere, Detectors and Associated Equipment **987**, 164833 (2021); <https://doi.org/10.1016/j.nima.2020.164833>
- [2] Y. Shu, J. Yan, Q. Lu, Z. Ji, D. Jin, Q. Xu, X. Hu, Sensors and Actuators B: Chemical **307**, 127593 (2020); <https://doi.org/10.1016/j.snb.2019.127593>
- [3] H. Li, X. Du, L. Cao, X. Guo, Z. Yuan, J. Matter Sci. **55**, 2905 (2020); <https://doi.org/10.1002/ppul.24734>
- [4] B. Barman, K. C. Handique, Y. Nanung, P. K. Kalita, Mater. Today: Proceed. **46**, 6213 (2021); <https://doi.org/10.1016/j.matpr.2020.04.658>
- [5] N. Suriyawong, R. Rajendran, C. Y. Hsieh, R. J. Wu, M. W. Lee, Sustain. Ener. Fuels **4**, 4859 (2020); <https://doi.org/10.1039/D0SE00839G>
- [6] S. K. Haram, K. S. V. Santhanam, Thin Solid Films **238**, 21 (1994); [https://doi.org/10.1016/0040-6090\(94\)90642-4](https://doi.org/10.1016/0040-6090(94)90642-4)

- [7] K. Kaviyarasu, A. Ayeshamariam, E. Manikandan, J. Kennedy, R. Ladchumananandasivam, U. U. Gomes, M. Jayachandranm, M. Maaza, Mater. Sci. Engin. B **210**, 1 (2016);
<https://doi.org/10.1016/j.mseb.2016.05.002>
- [8] R. B. Shafizade, I. V. Ivanova, M. M. Kazinets, Thin Solid Films **55**, 211 (1978);
[https://doi.org/10.1016/0040-6090\(78\)90051-2](https://doi.org/10.1016/0040-6090(78)90051-2)
- [9] S. R. Alharbi, A. F. Qasrawi, Physica E **125**, 114386 (2021);
<https://doi.org/10.1016/j.physe.2020.114386>
- [10] S. Namsani, B. Gahtori, S. Auluck, J. K. Singh, J. Comput. Chem. **38**, 2161 (2017);
<https://doi.org/10.1002/jcc.24865>
- [11] E. B. Watson, D. J. Chemiak, J. M. Hanchar, T. M. Harrison, D. A. Wark, Chem. Geol. **141**, 19 (1997); [https://doi.org/10.1016/S0009-2541\(97\)00054-5](https://doi.org/10.1016/S0009-2541(97)00054-5)
- [12] N. N. Kolesnikov, M. P. Kulakov, V. N. Molchanov, I. F. Schegolev, R. P. Shibaeva, V. I. Simonov, R. A. Tamazyan, O. M. Vyavilev, Physica C: Superconductivity **242**, 385 (1995);
[https://doi.org/10.1016/0921-4534\(94\)02420-0](https://doi.org/10.1016/0921-4534(94)02420-0)
- [13] X. Lin, J. C. Lu, Y. Shao, Y. Y. Zhang, X. Wu, J. B. Pan, L. Gao, S. Y. Zhu, K. Qian, Y. F. Zhang, D. L. Bao, L. F. Li, Y. Q. Wang, Z. L. Liu, J. T. Sun, T. Lei, C. Liu, J. O. Wang, K. Ibrahim, D. N. Leonard, W. Zhou, H. M. Guo, Y. L. Wang, S. X. Du, S. T. Pantelides, H. J. Gao, Nat. Mater. **16**, 717 (2017); <https://doi.org/10.1038/nmat4915>
- [14] S. R. Alharbi, A. F. Qasrawi, physica status solidi (a) **216**, 1800977 (2019);
<https://doi.org/10.1002/pssa.201800977>
- [15] N. M. Khusayfan, H. K. Khanfar, Results Phys. **12**, 645 (2019);
<https://doi.org/10.1016/j.rinp.2018.11.099>
- [16] F. Rong, Y. Bai, T. Chen, W. Zheng, Mater. Res. Bull. **47**, 92 (2012);
<https://doi.org/10.1016/j.materresbull.2011.09.026>
- [17] F. Monjezi, F. Jamali-Sheini, R. Yousefi, Sol. Energy **171**, 508 (2018);
<https://doi.org/10.1016/j.solener.2018.06.082>
- [18] S. Nakamura, T. Maeda, T. Wada, Jpn. J. Appl. Phys. **49**, 121203 (2020).
- [19] M. Zakria, A. Mahmood, A. Shah, Q. Raza, E. Ahmed, Progress in Natural Science: Materials International **22**, 281 (2012); <https://doi.org/10.1016/j.pnsc.2012.07.006>
- [20] J. I. Pankove, 1975 Optical processes in semiconductors. (New Jersey: Courier Corporation).
- [21] S. E. AlGarni, A. F. Qasrawi, Phys. Scripta **95**, 065801 (2020); <https://doi.org/10.1088/1402-4896/ab7c78>
- [22] A. Omar, A. F. Qasrawi, Physica Status Solidi B **257**, 1900711 (2020);
<https://doi.org/10.1002/pssb.201900711>
- [23] O. Madelung, 2004 Semiconductors: data handbook. (Berlin Heidelberg: Springer Science & Business Media); <https://doi.org/10.1007/978-3-642-18865-7>
- [24] A. Hofmann, C. Pettenkofer, Phys. Rev. B **84**, 115109 (2011);
<https://doi.org/10.1103/PhysRevB.84.064414>
- [25] A. F. Qasrawi, A. N. A. Ghannam, Mater. Res. Express **6**, 116412 (2019);
<https://doi.org/10.1088/2053-1591/ab444e>
- [26] A. F. Qasrawi, H. K. Khanfar, IEEE Sens. J. **20**, 14772 (2020);
<https://doi.org/10.1109/JSEN.2020.3009986>
- [27] T. S. Kayed, A. F. Qasrawi, Current Appl. Phys. **20**, 114 (2020);
<https://doi.org/10.1016/j.cap.2019.10.015>
- [28] I. G. Shitu, Z. A. Talib, J. L. Y. Chi, M. M. A. Kechick, H. Baqiah, Results Phys. **17**, 103041 (2020); <https://doi.org/10.1016/j.rinp.2020.103041>
- [29] Y. C. Lin, G. B. Rayner, J. Cardenas, A. D. Franklin, Appl. Phys. Lett **118**, 101903 (2021);
<https://doi.org/10.1063/5.0030555>
- [30] K. D. Kim, Y. J. Kim, M. H. Park, H. W. Park, Y. J. Kwon, Y. B. Lee, C. S. Hwang, Thin Film Adv. Funct. Mater. **29**, 1808228 (2019); <https://doi.org/10.1002/adfm.201905968>
- [31] M. Bansal, H. Kaur, 2018 Performance investigation of Negative Capacitance Germanium Double Gate-pFET (NCGe-DG-pFET) for improved analog applications 2018 International Symposium on Devices, Circuits and Systems (ISDCS);
<https://doi.org/10.1109/ISDCS.2018.8379686>